Journal of the Meteorological Society of Japan, Vol. 80, No. 4B, pp. 925–938, 2002

Vertical Wave Number Spectrum of Temperature Fluctuations in the Stratosphere using GPS Occultation Data

Toshitaka TSUDA

Radio Science Center for Space and Atmosphere (RASC), Kyoto University, Uji, Japan

and

Klemens HOCKE

Communications Research Laboratory (CRL), Tokyo, Japan

(Manuscript received 24 July 2001, in revised form 12 March 2002)

Abstract

We have analyzed small-scale fluctuations of temperature in the stratosphere using radio occultation data from the GPS/MET (GPS/Meteorology) experiment. From this, we have determined a vertical wave number spectrum of the normalized temperature fluctuations (T'/T) at 20–30 km and 30–40 km during three periods in June/July 1995, October 1995 and February 1997. The spectra at 20–30 km in the equatorial region in February 1997 agreed very well with radiosonde results in Indonesia as well as with a model spectrum assuming a linear saturation of gravity waves. We have found that the GPS radio occultation technique could measure meso-scale temperature perturbations in the lower stratosphere with a vertical wavelength down to 400 m. We have investigated the dependence of the mean wave number spectra on latitude, height and season. At 20–30 km the power law index for short wavelengths (<2 km) was about −3, consistent with a saturated gravity wave model. However, the spectral density was sometimes smaller than that predicted by the model. At 30–40 km both the spectral slope and density agreed well with the model for wavelengths shorter than about 1.5 km, though the slope was more gradual for small m. We have calculated the variance $(T'/T)^2$ integrating the spectra in two vertical wavelength ranges: 10–2.5 km and 2–0.4 km, and estimated potential energy per unit mass (Ep). Seasonal and latitudinal variations of Ep were evident at 20–30 km, in particular, Ep was highly enhanced near the equator for both long and short wavelength ranges. At 30–40 km the enhancement of Ep at low latitudes became less evident than at 20–30 km.

1. Introduction

It is now widely recognized that atmospheric gravity waves play a very important role in middle atmosphere dynamics. Gravity wave behavior has been studied by using data-sets collected with ground-based and satellite remote-sensing techniques as well as in-situ measurements. MST (mesosphere-stratosphere-troposphere) radars and lidars have provided detailed time and height structures of gravity waves in the troposphere and middle atmosphere, by taking advantage of their high resolution, continuous observations. These techniques are utilized, for example, to describe the characteristics of wind velocity and temperature fluctuations in terms of frequency and vertical wave number spectrum (e.g., Tsuda et al. 1994). However, geographical var-

Corresponding author: Toshitaka Tsuda, Radio Science Center for Space and Atmosphere (RASC), Kyoto University, Uji, Kyoto 611-0011, Japan.
E-mail: tsuda@kurasc.kyoto-u.ac.jp

iations of the gravity wave characteristics, which are crucial in estimating the wave forcing on the general circulation, are difficult to establish with the ground-based techniques, since observation sites are limited in number.

The latitude distribution of gravity wave activity in the stratosphere was first studied by Hirota (1984) by using routine meteorological rocketsonde data. The analysis was further expanded for long-term meteorological rocket soundings, mostly distributed in the northern hemisphere, to describe the seasonal and geographical variability of temperature and horizontal wind velocity fluctuations at 20–60 km caused by gravity waves (Hamilton 1991; Eckermann et al. 1995). These studies clarified that at middle and high latitudes the gravity wave activity showed a clear annual variation with a maximum in winter, consistent with MST radar observations (Murayama et al. 1994).

Horizontal distribution of meso-scale disturbances was studied using measurements from satellites equipped with LIMS (Limb Infrared Monitor of the Stratosphere) (Fetzer and Gille 1994). Wu and Waters (1996a,b) analyzed a global morphology of radiance fluctuations with a horizontal scale smaller than about 100 km in the upper stratosphere and mesosphere (30–80 km) from high-resolution measurements with the Microwave Limb Sounder (MLS) on board the Upper Atmosphere Research Satellite (UARS). A recent study by Jiang and Wu (2001) further clarified dependence of the radiance fluctuations on viewing angle of MLS as well as the effects of Doppler shifting by the background winds. Using the UARS/MLS data with a horizontal resolution of about 15 km, McLandress et al. (2000) also determined seasonal and geographical distributions of gravity waves, having vertical wavelengths longer than about 20 km.

Temperature fluctuations with short vertical wavelengths and relatively large horizontal scale were observed with CRISTA (Cryogenic Infrared Spectrometers and Telescopes for the Atmosphere) aboard the space shuttle (Eckermann and Preusse 1999; Preusse et al. 1999). Using high resolution temperature profiles obtained by the GPS/MET (Global Positioning System/ Meteorology) experiment, Tsuda et al. (2000) determined a global distribution of gravity wave potential energy per unit mass ($Ep = 1/2(g/N)^2(T'/T)^2$) with a vertical wavelength ranging from about 1.5 km to 10 km. Preusse et al. (2000) showed that the latitudinal distribution of Ep at 25–40 km was consistent between the CRISTA and GPS/MET results, showing large Ep at low latitudes, therefore, active wave generation by tropical convection was suggested. At higher altitudes, a latitude region of enhanced wave activity shifted toward middle and high latitudes of the winter hemisphere. Large Ep in the equatorial stratosphere was also recognized in rocketsonde (Eckermann et al. 1995) and radiosonde (Allen and Vincent 1995) studies.

Eckermann et al. (1995) clarified that wave energy at 20–40 km in the tropics could be contaminated by Kelvin waves and other equatorial waves. A recent study by Holton et al. (2001) reported the existence of a Kelvin wave with a vertical wavelength of about 5 km, therefore, the observed Ep in the tropics could include the effects of such waves. One of the major purposes of this study using GPS/MET data is to determine latitude dependence of temperature variance, having vertical wavelengths shorter than about 2 km, which is mostly contributed by gravity waves.

Since temperature and wind velocity fluctuations appear as a superposition of many gravity waves with various temporal and spatial scales, they may be described by a continuum spectrum in terms of frequency (ω), vertical and horizontal wave numbers (m and k, respectively). In particular, the observed vertical wave number spectrum for meso-scale fluctuations of both temperature and horizontal wind velocity are commonly approximated by m^{-3} for large m (Fritts et al. 1988; Tsuda et al. 1989, 1991; Allen and Vincent 1995). Several theoretical models have been proposed to explain the observed universal spectral shape (e.g., Smith et al. 1987; Hines 1991).

In particular, assuming wave breaking by convective instability, Smith et al. (1987) showed that at large m the saturation limit of the spectral density is determined by the atmospheric stability. Fritts and VanZandt (1993) employed the m spectrum proportional to

$$A(\mu) = A_0\mu^s/(1+\mu^{s+t}), \quad (1)$$

which was originally introduced as a model

of the oceanic wave field by Desaubies (1976). Here, A_0 is a normalization factor and $\mu = m/m^*$, where m^* is the characteristic wave number. Note that s and t are a constant, and t is normally assumed as 3. A saturated spectrum for the normalized temperature perturbations (T'/T) can be approximated as

$$F_{T'/T}(m) = N^4/(10g^2m^3), \quad (2)$$

for $m \gg m^*$, where N and g are the Brunt-Vaisala frequency and acceleration of gravity, respectively (Tsuda et al. 1991). While, for $m \ll m^*$ the spectral slope becomes flat or slightly positive, depending on s.

Tsuda et al. (1991) tested Eq. (2) for observed spectra obtained from campaign radiosonde soundings with a height resolution of 150 m at Shigaraki, Japan (35°N, 136°E). The observed spectral density in the lower stratosphere (18.5–25 km) in winter months exceeded the model prediction by factors of 1.3 to 1.9, and the power law index ranged from −2.9 to −3.2, indicating usefulness of the model. In the summer stratosphere, however, the spectral density was about half that predicted by the model, with the spectral slope ranging from −2.2 to −2.4. A climatological study of the temperature spectra in the lower stratosphere, using high-resolution routine balloon soundings over Australia, indicated that the spectral density was consistent overall with Eq. (2), while the spectral slope was about −2.5, slightly shallower than the model prediction (Allen and Vincent 1995).

Taking advantage of the high-resolution GPS/MET profiles, Steiner and Kirchengast (2000) analyzed a vertical wave number spectrum of temperature perturbations, which had been difficult to determine by conventional satellite measurements with a coarse height resolution. Using a few hundred GPS/MET occultation data collected on October 20 and 21, 1995, they showed that for wavelengths longer than about 2–5 km the analyzed spectra were generally consistent with a model spectrum of saturated gravity waves (Smith et al. 1987). The spectral density at low latitudes (30°N–30°S) was twice as high as that at higher latitudes. Steiner and Kirchengast, however, reported that the published GPS/MET data underestimate the spectral density for vertical wavelengths shorter than 2 km.

In this paper we first optimize our data analysis for recovery of the temperature profile, aiming at defining and improving the accuracy and height resolution of the GPS/MET profiles. We retrieve temperature profiles from the GPS phase signals (Level-2 data) by adjusting analysis parameters. Then, we determine a vertical wave number spectrum of T'/T in the stratosphere, and compare it to nearby radiosonde results and a model spectrum. We also discuss the sensitivity of the radio occultation technique for small-scale atmospheric fluctuations. Further, we investigate latitude variations of the spectra at 20–30 km and 30–40 km during three selected time periods of higher GPS signal quality ("prime times"), collected in June/July 1995, October 1995 and February 1997. Note that during a prime time both anti-spoofing (A/S) encryption and selective availability of the GPS system were turned off for the GPS/MET experiment in order to enable a higher precision of GPS atmosphere profiling.

2. Retrieval of temperature profiles with the GPS occultation technique

2.1 Outline of the GPS / MET experiment

The GPS/MET (Global Positioning System/Meteorology) project, initiated by UCAR (University Corporation for Atmospheric Research), launched a GPS receiver aboard a small satellite (Microlab-1) on April 3, 1995, into a low earth orbit (LEO) (Ware et al. 1996). The receiver recorded phase path delays of signals from GPS satellites setting behind the Earth's limb. This measurement technique is called radio occultation or active GPS limb sounding. By applying the Abel transform, height profiles of atmospheric refractive index were obtained in the troposphere, middle atmosphere and ionosphere from April 1995 to February 1997 (Rocken et al. 1997). A new global data set of high-resolution profiles of temperature, humidity and electron density has been generated by the GPS/MET mission. In particular, by assuming the hydrostatic relation for a dry atmosphere, temperature is determined with high accuracy in the upper troposphere and stratosphere (from 5–10 to 60 km) (Rocken et al. 1997).

The accuracy of the radio occultation technique has been studied, considering a variety of possible errors (Kursinski et al. 1997). Com-

paring a GPS/MET temperature profile with a nearby radiosonde sounding, Nishida et al. (2000) reported that GPS/MET can detect a detailed temperature profile including a sharp temperature inversion around the tropical tropopause. Rocken et al. (1997) conducted a validation study of GPS/MET temperature profiles and compared them with data from other independent sources, such as radiosondes and other satellite measurements as well as model analyses. The rms temperature difference was found to be about 1 K in the upper troposphere and increased to 2 K in the stratosphere. The increase was partially attributed to spatial variations of temperature fluctuations caused by atmospheric waves (Tsuda et al. 2000). Recently, Palmer and Barnett (2001) and Gorbunov and Kornblueh (2001) demonstrated the usefulness of GPS occultation data by comparing the GPS/MET results with numerical weather prediction models.

2.2 *Optimization of bending angle profile*

The fundamental principle of occultation measurement with GPS radio signals is related to the determination of bending angle (α) of the propagation ray path as a function of the tangent height of the ray (Ware et al. 1996). Then, α can be converted to a refractive index profile, which is related to atmospheric parameters, such as temperature, pressure and humidity.

We describe here an optimization procedure of α. First, the observed bending angle (α_o) is used without correction below 30 km. A model profile (α_m) is defined by using MSISE-90 (Mass Spectrometer and Incoherent Scatter Extended atmospheric model) (Hedin 1991) above 30 km, where α_m is smoothly connected to α_o at 30 km. Above 70 km α_m is used without referring to α_o. Between 30 and 70 km, α is optimized by comparing α_o and α_m in order to suppress noise. Sharp gradients of the bending angle profile due to noise can introduce serious errors or a failure of the subsequent temperature retrieval via inverse Abel transform. To avoid such errors, deviations of α_o from α_m are controlled and reduced by calculating the weighted means between α_o and α_m, where a weighting function is defined as

$$W = 1/(1 + |\alpha_o - \alpha_m|/0.2\alpha_m). \quad (3)$$

As a result, amplitudes of the α fluctuations are somewhat suppressed. For example, the weighting coefficient (W) becomes 0.5 for a 20% difference.

We have derived a vertical profile of W for 82 GPS/MET occultation data on July 3, 1995 during a prime time. We have found that W was nearly constant at 0.7–0.8 at 30–40 km. This means that any deviation of α_o, consisting of both stationary and fluctuating components, are reduced by 5–8.6% at 30–40 km. Note that we are unable to separately estimate the reduction rate of α_o between the mean and perturbation components, where the latter is presumably caused by gravity waves. Above 40 km W rapidly decreased, which indicates that deviations of the resultant α from α_m were significantly suppressed.

We have also analyzed 98 events on October 23, 1996 under A/S-on conditions. It has been reported that with A/S-on the effects of ionospheric correction could produce artificial fluctuations in the GPS/MET profiles down to about 30 km due to low SNR of the L2 band of GPS signal (Rocken et al. 1997). We have found that W linearly decreased from 0.75 at 30 km to 0.3 at 50 km, which indicates that the height structure of α may not fully reflect actual atmospheric phenomena even below 40 km.

To summarize, we have restricted our analysis of stratospheric gravity waves to the GPS/MET data during the prime time and below 40 km.

3. Analysis of $F_{T'/T}(m)$ using GPS/MET data

3.1 *Comparison of $F_{T'/T}(m)$ between GPS/MET, radiosonde and model results*

From Level-2 data of GPS/MET we have retrieved temperature profiles by changing the data smoothing range, which is related to the height resolution of the profiles. Smoothing of the time series of the phase path was performed by a sliding cubic polynomial fit (including singular value decomposition). Within this procedure the time derivative of the phase path delay is also obtained, which is used for calculation of Doppler frequency shift and bending angle. In the following, the number of points of the data window of the polynomial fit is called N_{ASOFF}, where ASOFF stands for "anti-spoofing off". Note that we have used a retrieval algorithm developed by Hocke (1997),

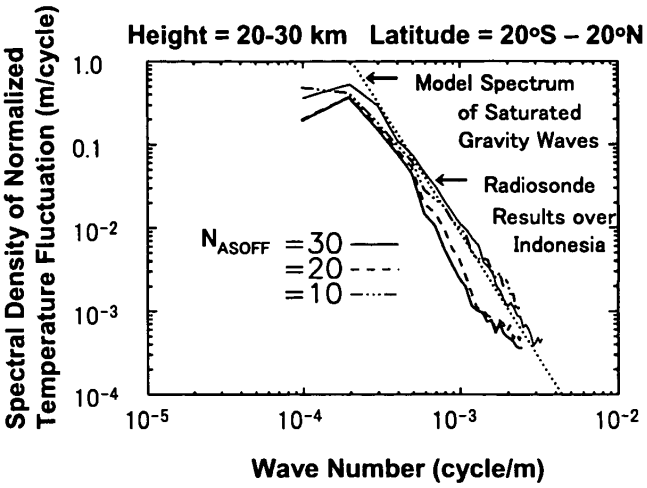

Fig. 1. Vertical wave number spectrum of the normalized temperature fluctuations at 20–30 km from GPS/MET data collected in a latitude band from 20°N to 20°S in February, 1997. Thick-solid, dashed and chained lines correspond to the spectra from GPS/MET temperature retrievals with the number of smoothing data points (N_{ASOFF}) of 30, 20 and 10, respectively (Hocke, 1997). The dotted line indicates a model spectrum of saturated gravity waves, shown in Eq. (2) (Smith et al. 1987). The thin-solid line shows an average spectrum from 78 radiosonde soundings at Pontianak (0°, 109°E), Indonesia in January–February 1997.

whose basic algorithm is similar to that used at UCAR (Rocken et al. 1997).

From temperature fluctuations evident in the retrieved temperature profiles, $T'(z)$, we have computed and analyzed power spectral densities of normalized temperature fluctuations (T'/T). Figure 1 shows a vertical wave number spectrum of (T'/T) at 20–30 km by using GPS/MET data collected during a prime time on February 2–10, 1997. Note that m in Fig. 1 corresponds to 1/(vertical wavelength), not 2π/(vertical wavelength), thus, its unit becomes cycles/m. The smoothing range of phase data (N_{ASOFF}) was set equal to 10, 20 and 30, where $N_{ASOFF} = 30$ nearly corresponds to the results published by the GPS/MET office at UCAR. We have averaged 83 spectra obtained in a latitude range from 20°N to 20°S. The spectral density agreed well for $m = 2–5 \times 10^{-4}$ (cyc/m) between the three determinations. Note that the first spectral point was affected by a window function used in the spectral analysis, therefore, it is less significant. For $m < 5 \times 10^{-4}$ (cyc/m) the spectral density with $N_{ASOFF} = 30$ and 20 was depressed compared to that with $N_{ASOFF} = 10$.

The spectra are compared in Fig. 1 with a radiosonde result from the tropics. The thin solid line corresponds to a mean spectrum for 78 soundings, with a height resolution of about 100 m, obtained during a campaign observation at Pontianak (0°, 109°E), Indonesia from January to February, 1997. We also show in Fig. 1 a model spectrum defined by Eq. (2) for large m (Smith et al. 1987).

The GPS/MET spectrum with $N_{ASOFF} = 10$ agrees very well with both the radiosonde result and the saturated model spectrum particularly for large m. On the other hand, the spectral density for the other two GPS/MET spectra differ significantly for $m < 5 \times 10^{-4}$ (cyc/m). Figure 1 suggests that GPS/MET can measure gravity waves with a vertical wavelength down to about 400 m at 20–30 km altitude.

Applying the same procedure, we have analyzed vertical wave number spectra at 30–40 km and 40–50 km as shown in Fig. 2. At 30–40 km the spectrum with $N_{ASOFF} = 10$ agrees well with a theoretical saturation limit for large m. However, the spectral density seems to become smaller than the model prediction for small m. At 40–50 km observed spectral density exceeded a theoretical model probably due to spurious temperature fluctuations caused by ionospheric correction and receiver noise. Therefore, the spectra at 40–50 km were not used in the following analysis.

3.2 *Height resolution of GPS occultation measurements*

In the previous section we have investigated how far the small scale part of the vertical wave number spectra observed by GPS/MET can be used for meteorological studies. We have shown that the observed spectral slopes and spectral density of the vertical wave number spectra are consistent with model predictions of saturated gravity wave spectra. However, we do not clearly define the resolution of the GPS occultation measurements, because the above conclusions mainly rely on an empirical test. In the following, we discuss the resolution of GPS

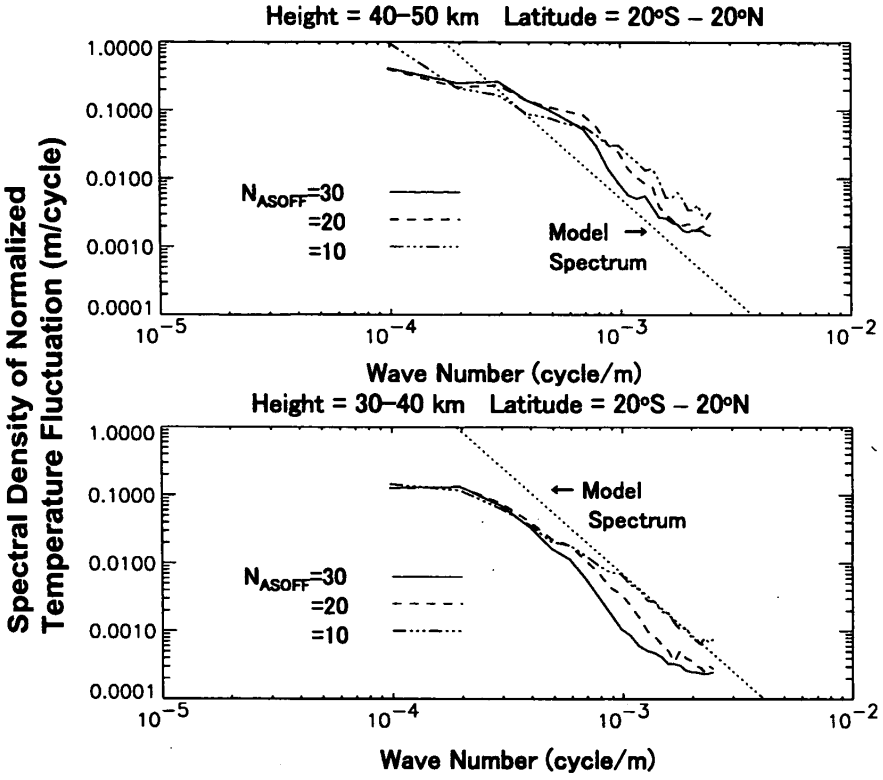

Fig. 2. The same as Fig. 1 except for the GPS/MET spectra at 40–50 km (top) and 30–40 km (bottom).

occultation measurements of small-scale fluctuations. Coherent weak scattering of GPS signals by atmospheric irregularities is assumed to explain the sensitivity of GPS radio occultation at small scales.

For a radio occultation measurement the GPS receiver on the LEO satellite selects a radio link to a GPS satellite setting behind the Earth's limb. The effective sounding volume can be described as a tube with a diameter of around 1 km and a length of less than a few hundreds kilometers. This tube is elongated along the radio ray from the LEO to the GPS satellite and centered at the ray tangent point, which is the point of closest approach of the radio link to the Earth's center. The movement of the sounding volume (or tangent point) inside the atmosphere during a radio occultation mainly depends on the angle between the velocity vector of the LEO satellite and the radio link vector, that is, the vector pointing from LEO to the GPS satellite.

The GPS/MET mission favored the sounding of the atmospheric limb in the anti-velocity direction of the Microlab-1 satellite. In this case the tangent point moves downward through the atmosphere, with a vertical velocity of around 2.5–3 km/s. The GPS receiver records spatial and vertical irregularities of the atmosphere as temporal fluctuations of the signal-to-noise ratio and phase path excess of the GPS signal. The sampling frequency of the GPS/MET experiment is 50 Hz, and so it is possible to resolve fluctuations with frequencies less than the Nyquist frequency of 25 Hz, corresponding to irregularities with vertical wavelengths > 100 m (=2.5 km/s/25 Hz).

The phase path fluctuations are mainly generated at the ray tangent point, while GPS amplitude fluctuations are generated by atmospheric irregularities along the whole ray path (Haugstad 1981; Hinson and Tyler 1983). In the present study we derive the temperature profile from the measurement of phase path excess, and fluctuations of phase path are inverted into temperature fluctuations.

For interpretation of the vertical wave number spectra of the temperature profiles we keep in mind that the spectra can be influenced by several effects. The most important are (1) the effect of anisotropic irregularity distribution on absolute value and spectral slope of the power

spectrum, (2) underestimation of small scale horizontal variations due to "smoothing out" along the ray path tube, and (3) the Fresnel filtering effect on irregularities with scales comparable to or less than the first Fresnel zone diameter, which is around 1.4 km for GPS/MET observations at stratospheric heights. Atmospheric structures with vertical wavelengths similar to the Fresnel zone diameter can be emphasized in the power spectrum. This is due to interference effects of the GPS radio wave field after passing atmospheric irregularities at the Earth's limb (Karayel and Hinson 1997). Averaging of many GPS/MET spectra significantly diminishes the influence of the three critical effects mentioned above.

Earlier studies by the planetary science community gave evidence that radio occultation spectra can provide quantitative estimates of atmospheric wave distribution, turbulence (sub-Fresnel zone range), and anisotropy of irregularities for various planets of our solar system (e.g., Hinson and Tyler 1982, 1983; Haugstad 1981). Using a weak scattering theory and a phase screen approach, these scientists developed a data analysis method to derive the complete vertical wave number spectra observed during planetary occultation measurements by the Mariner, Pioneer and Voyager missions. Detailed description of the small-scale irregularity distribution of the Earth's atmosphere will be feasible by collection of more GPS radio occultation data and by more advanced data analysis and validation.

4. Seasonal and latitudinal variations of $F_{T'/T}(m)$ at 20–40 km

Figure 3 shows variations of vertical wave number spectra with season and latitude at 20–30 km. For this study Level-2 data were available during three prime time periods: October 10–25, 1995, June 19–July 10, 1995 and February 2–16, 1997, which could represent atmospheric conditions for an equinox and two

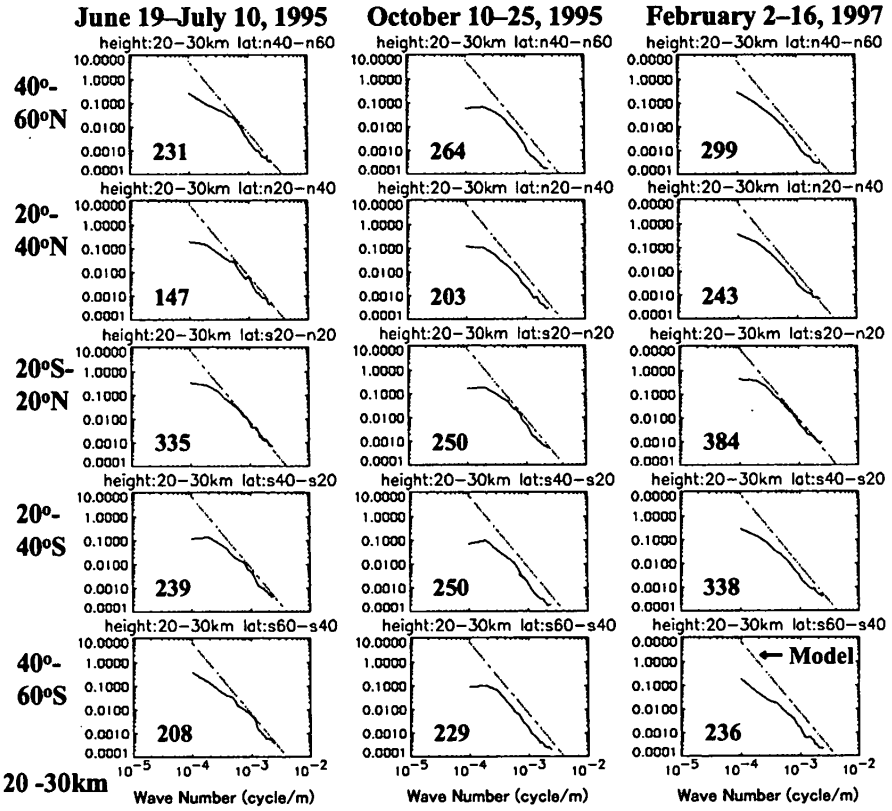

Fig. 3. Vertical wavenumber spectrum of T'/T at 20–30 km from GPS/MET data in three prime times; June 19–July 10, 1995 (left), October 10–25, 1995 (center) and February 2–16, 1997 (right). From top to bottom rows the latitude range of the analysis corresponds to 40°–60°N, 20°–40°N, 20°N–20°S, 20°–40°S, 40°–60°S, respectively. Each panel shows the number of GPS/MET profiles as well as a saturated spectrum model by using the observed N^2.

solstices, respectively. We have selected five latitude ranges (i.e., 40°N–60°N, 20°N–40°N, 20°N–20°S, 20°S–40°S, 40°S–60°S), but we discarded data at latitudes higher than 60°, since the amount of data available rapidly decreases there. We have analyzed a total of about 1200–1500 spectra taken during each prime time, and determined a mean spectrum by arithmetically averaging about 150–380 spectra indicated in each panel of Fig. 3. Although we also analyzed data from another prime time from April 21 to May 5, 1995, only 320 profiles were available from this time period, and the mean spectra show considerable fluctuation. Consequently, the results are not included in this study, as they are statistically less significant.

In each panel in Fig. 3, a theoretical saturation limit for large wave numbers defined by Eq. (2) is also plotted, where the background N^2 is determined from the GPS/MET temperature profiles in the corresponding season and latitude range.

In the equatorial region (20°N–20°S), the observed spectra in the three periods agreed very well with the model for $m > 5 \times 10^{-4}$ (cyc/m), showing a power law index (logarithmic slope) of about −3. The observed spectra tended to differ from the m^{-3} form for small m, which is consistent with earlier ground-based studies (Tsuda et al. 1991; Allen and Vincent 1995). Although a dominant vertical wavelength of gravity waves cannot clearly be identified from a breakpoint of the spectra (Fritts et al. 1988), it seems to be as long as about 5 km. We estimated a power law index of each spectrum in Fig. 3 in a wave number range from 5.88×10^{-4} to 1.86×10^{-3} (cyc/m) (1.7–0.54 km in wavelength), and summarized in Table 1. Overall average of the estimated slope was −3.04, which is very close to the model prediction.

At extra-tropical latitudes (20°–60°N and 20°–60°S) the spectral density observed in June–July, 1995 was very close to the saturation limit for large m. However, discrepancy between observations and the model becomes larger for small m, which was more evident at high latitudes.

In October, 1995, the asymptotic slope of the observed spectra at 20°–60°N and 20°–60°S ranged −3.0 to −3.4, and the spectral shape was consistent with the model, but the spectral density for large m was only about half of that predicted by the model. Note that the theoretical saturation limit is calculated by using the observed N^2, which does not explain the suppression of the spectral density for large m. The dominant vertical wavelength at 40°–60°N and 40°–60°S can be inferred as about 3 km.

Figure 4 shows the observed spectra at 30–40 km in the same format as in Fig. 3. The spectral slope is gradual for $m < 1 \times 10^{-3}$ (cyc/m), that is, the spectral density was somewhat smaller than the saturation limit. However, the spectra for large m are consistent with Eq. (2). In Table 1, we also summarize a power low index of the spectra in Fig. 4. Note that we estimated the slope in two wave number ranges: (a) from 9.80×10^{-4} to 2.06×10^{-3} (cyc/m) (1.02–0.49 km) and (b) from 3.92×10^{-4} to 8.82×10^{-4} (cyc/m) (2.55–1.13 km). The spectral density more closely approached the theoretical limit than that at 20–30 km, though it was sometimes smaller than the model, particularly at 20°–60°S in October, 1995.

5. Latitudinal variations of stratospheric gravity wave energy

5.1 *Latitude variations of Ep from GPS/MET results*

We have calculated the variance of the normalized temperature perturbations $(T'/T)^2$, at 20–30 km and 30–40 km, integrating the spectra in Figs. 3 and 4, respectively, in long (10–2.5 km) and short (2–0.4 km) vertical wavelength ranges. Then, the wave potential energy per unit mass (Ep) is calculated by using the observed N^2 in each height range. Latitude variations of E_p in the three observation periods are shown in Fig. 5. Note that $(T'/T)^2$, E_p and N^2 at 20–30 km and 30–40 km are also summarized in Tables 2 and 3, respectively.

Figure 5 (a) and (b) indicate that Ep in the two wavelength ranges was enhanced at 20°N–20°S by 2–4 times over that at 40°–60°N and 40°–60°S. Between 40°N and 40°S, Ep in Fig. 5 (a) for the long wavelength range was larger in February than in June, while that for the shorter range in Fig. 5 (b) was comparable between February and October. Ep was generally the smallest in October. At 40°–60°, Ep was larger in the winter hemisphere, though the hemispheric asymmetry was smaller for the short wavelength components.

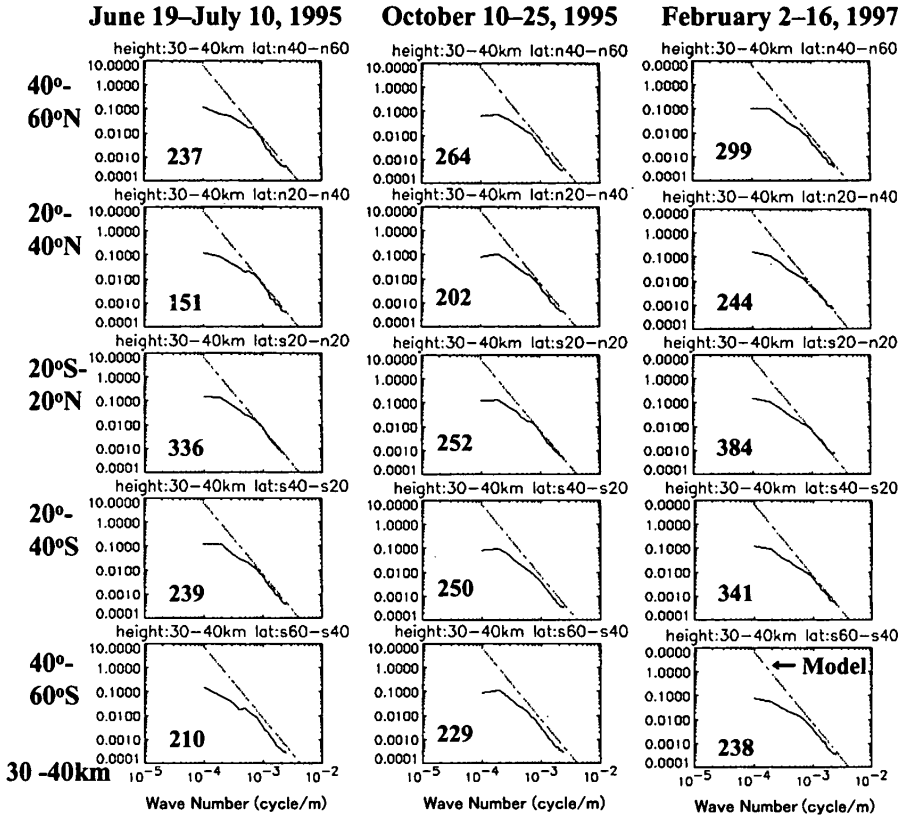

Fig. 4. The same as Fig. 3 except for the results at 30–40 km.

Table 1. Power law index of vertical wave number spectra at 20–30 km and 30–40 km. The index is estimated in a wave number range from 5.88×10^{-4} to 1.86×10^{-3} (cyc/m) (1.7–0.54 km in wavelength) at 20–30 km, while, at 30–40 km it is calculated in two wave number ranges: (a) from 9.80×10^{-4} to 2.06×10^{-3} (cyc/m) (1.02–0.49 km) and (b) from 3.92×10^{-4} to 8.82×10^{-4} (cyc/m) (2.55–1.13 km).

	June		October		February	
20-30km						
40°-60°N	-3.5		-3.4		-3.0	
20°-40°N	-3.1		-3.0		-2.7	
20°N-20°S	-2.9		-3.4		-2.8	
20°-40°S	-3.0		-3.4		-2.8	
40°-60°S	-2.9		-3.1		-2.8	
30-40km	(a)	(b)	(a)	(b)	(a)	(b)
40°-60°N	-3.5	-1.5	-3.2	-2.1	-2.9	-1.8
20°-40°N	-3.4	-1.3	-3.2	-1.8	-2.8	-1.6
20°N-20°S	-3.3	-1.6	-3.2	-1.8	-3.1	-1.5
20°-40°S	-3.3	-1.8	-3.2	-1.6	-3.1	-1.5
40°-60°S	-3.2	-1.7	-3.0	-1.5	-3.1	-1.7

In Fig. 5 (c) and (d) the *Ep* at low latitudes is 3.3–3.7 (J/kg) and about 1 (J/kg) for long and short wavelength ranges, respectively, which are smaller than those at 20–30 km by a factor of about 1/2 and 3/4, respectively. Although *Ep* at 30–40 km in Fig. 5 (c) also increased at low latitudes, the enhancement was moderate compared to that at 20–30 km. *Ep* for the 10–2.5 km components in Fig. 5 (d) showed a hemispheric asymmetry with larger values in winter. Moreover, *Ep* was smaller in the southern hemisphere, which does not show significant seasonal variations. *Ep* was generally smaller in October, except at 40°–60°S for the (10–2.5 km) components, though the difference was rather small.

In Table 2 we show latitudinal and seasonal variations of the background N^2 at 20–30 km determined using GPS/MET temperature profiles. N^2 reached a maximum in the equatorial region (20°N–20°S), and became smaller at 40°–60° by 12–17%, which causes a decrease of the theoretical saturation limit by a factor of 0.7–0.8. Seasonal variation of N^2 in each lati-

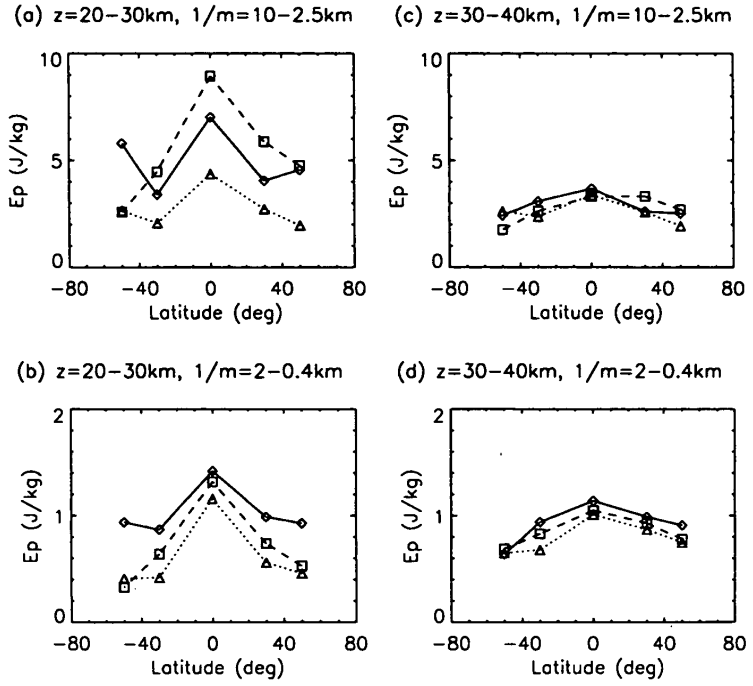

Fig. 5. Latitude variations of Ep at 20–30 km (left) and 30–40 km (right), calculated by integrating the temperature variance from spectra in Figs. 3 and 4. Top and bottom rows correspond to Ep in long (10–2.5 km) and short (2–0.4 km) vertical wavelength ranges. Solid line with diamond, dotted line with triangle and dashed line with square indicate the results in June, October and February, respectively.

Table 2. Latitude variations of N^2, $(T'/T)^2$ and E_p at 20–30 km estimated from the observed wave number spectra shown in Fig. 3 in two wavelengths ranges: 10–2.5 km and 2–0.4 km.

20–30 km	N^2 X10^{-4} (rad/s)^2	$(T/T)^2$ x10^{-5}	E_p J/kg	$(T'/T)^2$ x10^{-6}	E_p J/kg
June		10–2.5 km		2–0.4 km	
40°–60°N	4.64	4.39	4.55	8.97	0.93
20°–40°N	5.12	4.32	4.05	10.56	0.99
20°N–20°S	5.34	7.71	7.02	15.85	1.42
20°–40°S	5.21	3.68	3.39	9.43	0.87
40°–60°S	5.01	6.04	5.79	9.83	0.94
October		10–2.5 km		2–0.4 km	
40°–60°N	4.71	1.92	1.96	4.47	0.46
20°–40°N	5.23	2.96	2.72	6.04	0.56
20°N–20°S	5.51	5.01	4.37	13.25	1.16
20°–40°S	5.23	2.25	2.06	4.52	0.42
40°–60°S	4.95	2.72	2.64	4.18	0.41
February		10–2.5 km		2–0.4 km	
40°–60°N	4.64	4.60	4.76	5.10	0.53
20°–40°N	5.28	6.46	5.87	8.15	0.74
20°N–20°S	5.63	10.49	8.94	15.51	1.32
20°–40°S	5.53	5.13	4.46	7.41	0.64
40°–60°S	5.02	2.69	2.58	3.49	0.33

Table 3. Latitude variations of N^2, $(T'/T)^2$ and E_p at 30–40 km estimated from the observed wave number spectra shown in Fig. 4 in two wavelengths ranges: 10–2.5 km and 2–0.4 km.

30–40 km	N^2 x10^{-4} (rad/s)^2	$(T/T)^2$ x10^{-5}	E_p J/kg	$(T'/T)^2$ x10^{-6}	E_p J/kg
June		10–2.5 km		2–0.4 km	
40°–60°N	5.04	2.63	2.51	9.56	0.91
20°–40°N	5.08	2.75	2.60	10.52	0.99
20°N–20°S	5.09	3.89	3.67	12.04	1.14
20°–40°S	5.09	3.26	3.08	9.98	0.94
40°–60°S	5.41	2.72	2.42	7.23	0.64
October		10–2.5 km		2–0.4 km	
40°–60°N	5.13	2.07	1.93	7.98	0.75
20°–40°N	5.09	2.73	2.58	9.25	0.87
20°N–20°S	5.10	3.59	3.38	10.77	1.01
20°–40°S	5.15	2.53	2.36	7.25	0.68
40°–60°S	5.10	2.79	2.62	6.88	0.65
February		10–2.5 km		2–0.4 km	
40°–60°N	5.18	2.90	2.69	8.45	0.78
20°–40°N	5.25	3.62	3.31	10.21	0.93
20°N–20°S	5.12	3.51	3.30	11.15	1.05
20°–40°S	5.11	2.78	2.62	8.81	0.83
40°–60°S	5.06	1.84	1.75	7.28	0.69

tude band was less than 5%. Latitudinal and seasonal variations of N^2 at 30–40 km in Table 3 are less than 2%.

The latitude variations of Ep for the long wavelength components did not necessarily depend on those in N^2, because the wave amplitudes may not fully saturated. On the other hand, Ep for short wavelengths seemed to be related to N^2, considering Eq. (2). However, the enhancement of Ep near the equator was much larger than the latitude variation of N^2. Therefore, the linear saturation theory of gravity wave does not completely explain the wave amplitudes for small vertical wavelengths, although the asymptotic logarithmic slope of the observed spectra is described well by the model in Figs. 3 and 4.

5.2 *Effects of observation filter on Ep*

Because the GPS/MET temperature profile is retrieved from the limb occultation measurement of GPS radio signals by assuming a spherical symmetry, it smears out details of the horizontal structure within a sample volume. Therefore, the GPS/MET data cannot resolve gravity waves with a large horizontal wave number. As a result, the observed vertical wave number spectrum may also be modified, since it is linked to a horizontal wave number spectrum through a dispersion relation.

Alexander (1998) reported that the cutoffs in the observed spectra caused by the scale selectivity of each measurement technique produce a number of problems and misinterpretations of gravity wave variance measured by limb-viewing instruments. McLandress et al. (2000) analyzed a global distribution of temperature variance with UARS/MLS, considering the effects of the observational filter, and found the significant effects by the background winds.

We investigate in the following the effects of the observation filter on Ep shown in Fig. 5. First, we estimate the shortest horizontal wavelength that can be resolved with GPS/MET. Neglecting the bending of a GPS ray path, the horizontal extent of a spherical shell with a thickness of d becomes

$$h_{\mathrm{GPS}} = 2(2d(r+z))^{1/2}, \tag{4}$$

where r is the Earth's radius (6,370 km) and z is the tangent height for the ray path of GPS signals. By substituting $d = 1.4$ km in Eq. (4) from the vertical scale of the first Fresnel diffraction pattern for a uniform refractive index profile, h_{GPS} becomes about 270 km. Similarly, h_{GPS} can be estimated as about 100 km for $d = 200$ m, which is inferred as the height resolution of GPS/MET in this study.

Next, we employ a 2-dimensional spectrum of linear gravity waves. Following Fritts and VanZandt (1993), we assume that the spectrum is separable as

$$F(m,\omega) = E_0 A(m) B(\omega), \tag{5}$$

in terms of m and wave frequency, ω. We assume here that $B(\omega)$ has a ω^{-p} form between the inertial frequency, f, and N, with p ranging from 5/3 to 2. $A(m)$ is described in Eq (1), but, for this preliminary analysis we assume a m^{-3} form shown in Eq (2) for simplicity. Note that we neglect azimuth dependence of the gravity wave field as well as the effects of the mean background winds for simplicity. By using a dispersion relation $|\omega = kN/m|$, the spectrum can be converted to

$$\begin{aligned} G(k,m) &= F(m,\omega)\, d\omega/dk \\ &= E_0 A(m) m^{p-1} N^{1-p} k^{-p}, \end{aligned} \tag{6}$$

as described in Gardner et al. (1993). Integrating $G(k,m)$ over an appropriate range of k, considering the spatial filter function of the occultation measurements, we could obtain a vertical wave number spectrum, $H(m)$, which is applicable for the GPS/MET results.

However, it is difficult to exactly quantify a reduction factor of $H(m)$ relative to the true spectrum, because the allowable range of horizontal wavelengths of gravity waves has not been clearly defined yet from observations. According to Gardner et al. (1993), the minimum horizontal wavelength (λ_{min}) can be assumed as 500 m, while, the maximum wavelength is delineated as

$$\lambda_{\mathrm{max}} = N/(m^* f). \tag{7}$$

With $m^* = 1/5$ km, $p = 5/3$ and $N = 2\pi/5$ min, λ_{max} can be inferred as about 1,500 km and 1,000 km at the 30° and 50° latitudes, respectively, which can be used as the representative value in the middle (20°–40°) and high (40°–60°) latitude regions. But, λ_{max} in the tropics is rather uncertain, because Eq. (7) predicts that λ_{max} rapidly increases at low latitudes

as f approaches zero toward the equator. Substituting f at the 10° latitude, we obtain $\lambda_{max} = 4{,}000$ km from Eq. (7), which is consistent with radiosonde results in Indonesia (Shimizu and Tsuda 1997).

For simplicity, we assume that the shape of the observation filter for the GPS/MET measurements is a rectangular box with zero power for wavelengths below h_{GPS}. Substituting these parameter in the integral, we can estimate the respective reduction factor at 50°, 30° and 10° latitudes as about 0.59, 0.68 and 0.84 with $h_{GPS} = 270$ km, and 0.76, 0.84 and 0.92 with $h_{GPS} = 100$ km. The observed $(T'/T)^2$ and E_p in Tables 2 and 3 and Fig. 5 could be underestimated by these factors due to the effects of the observation filter.

Table 3 indicates that latitude variations of E_p at 30–40 km for the (10–2.5 km) components are on average very close to the calculated reduction factor. However, for the (2–0.4 km) components the latitude decrease in E_p is larger than that for the long wavelength components, which is opposite to the above prediction. On the other hand, at 20–30 km we can obviously recognize a more significant enhancement of E_p in the tropics relative to E_p at 20°–40° and 40°–60°.

Note that these estimates are very preliminary by using a simplified spectral model. Therefore, we may need to develop a more sophisticated method in a future study, taking into account, for example, the Doppler shifting by the background winds and azimuth anisotropy of the gravity wave field. A recent study by Alexander et al. (2002) showed that the pronounced Ep at 18–25 km in the tropics, detected in the GPS/MET results with the 1.5–10 km wavelengths (Tsuda et al. 2000), can be explained by assuming a shallower frequency spectrum of gravity waves and intermittency of the wave generation.

It may be useful to briefly summarize here a comparison study on gravity wave energy between GPS/MET and MST radars (Nastrom et al. 2000; Tsuda et al. 2000). MST radars can accurately determine the kinetic energy per unit mass, E_k caused by gravity waves. So, climatological values of E_k with the MU radar (35°N) and the White Sands wind profiler (32°N) were compared with Ep determined for the 1.5–10 km wavelength components by using nearby GPS/MET profiles. Individual comparisons determined a ratio of E_k to Ep as 1.7 and 1.66, respectively, which is very close to p predicted by a linear gravity wave theory. Therefore, a possible reduction of Ep caused by the observation filter effects was not identified.

6. Concluding remarks

We have retrieved temperature profiles from Level-2 data of GPS/MET during three prime time periods under the A/S-off condition (June/July 1995, October 1995 and February 1997), using a smoothing range of the GPS phase signals which was shorter than a nominal value adopted for the published data from the UCAR GPS/MET office. We have analyzed a vertical wave number spectrum of T'/T, and investigated its dependence on latitude, height and season.

From a comparison of the analyzed spectra in February 1997 at 20–30 km in an equatorial region with nearby radiosonde results and a theoretical prediction using linear saturation theory, we have found that temperature fluctuations with a vertical wavelength down to 400 m have been accurately measured by the GPS occultation technique.

Amplitudes of temperature fluctuations at 30–40 km could be somewhat reduced through the optimization of the occultation analysis. We have investigated variations of vertical wave number spectra of $(T'/T)^2$ at 20–30 km and 30–40 km as a function of latitude and season.

At 20–30 km the power law index for short wavelengths (<2 km) was about −3 as predicted by a saturated gravity wave model. It is noteworthy, however, pseudo fluctuations with a sub-Fresnel scale could be produced in the retrieved temperature profiles (Karayel and Hinson 1997). Therefore, it is difficult to confirm whether the analyzed spectrum is entirely attributed to the gravity wave effects.

The spectral density was sometimes smaller than that given by the model. At 30–40 km both the spectral density and power law index agreed well with the model, especially for wavelengths shorter than about 1.5 km. But, the slope became mode gradual than −3 for wavelengths longer then 1.5 km, showing departure from the model.

Integrating the observed spectra for long (10–2.5 km) and short (2–0.4 km) vertical

wavelength ranges, we have calculated the variance of the normalized temperature perturbations $(T'/T)^2$. We, then, calculated the potential energy per unit mass (Ep) at 20–30 km and 30–40 km in each month. Seasonal and latitudinal variations of Ep were evident at 20–30 km. In particular, Ep was largely enhanced near the equator for both long (10–2.5 km) and short (2–0.4 km) wavelength ranges. The enhancement at low latitudes became less evident at 30–40 km. These variations were larger than those for the background N^2 values. Though the dependence of $(T'/T)^2$ on the background atmospheric stability is predicted as in Eq. (2) from a linear saturation theory, it does not seem to explain the latitude variation of gravity wave energy.

Assuming a simple model spectrum, we have investigated the observation filter effects caused by the horizontal scale selectivity of GPS limb occultation measurements, and estimated the latitude dependence in the reduction factor of Ep. The observed latitude distribution of Ep at 30–40 km for the (10–2.5 km) wavelengths is consistent with the model prediction. However, at 20–30 km Ep was more significantly enhanced in the tropics.

Acknowledgements

The GPS/MET program is sponsored primarily by the National Science Foundation (NSF). We greatly appreciate Drs. C. Rocken and D. Hunt at UCAR for providing us of GPS/MET Level-2 data collected during a prime time. This study is supported by the Japanese GPS Meteorology project of the Ministry of Education, Culture, Sports, Science and Technology (MEXT), Japan. We deeply thank Mr. M. Iwata for his assistance in analyzing the GPS/MET data. We appreciate very much the constructive comments provided by anonymous reviewers, which are very valuable in improving this paper.

References

Alexander, M.J., 1998: Interpretations of observed climatological patterns in stratospheric gravity wave variance, *J. Geophys. Res.*, **103**, 8627–8640.

———, T. Tsuda, and R.A. Vincent, 2002: On the latitude variations observed in gravity waves with short vertical wavelengths, *J. Atmos. Sci.*, **59**, 1394–1404.

Allen, S.J. and R.A. Vincent, 1995: Gravity wave activity in the lower atmosphere: Seasonal and latitudinal variations, *J. Geophys. Res.*, **100**, 1327–1350.

Desaubies, Y.J.F., 1976: Analytical Representation of Internal Wave Spectra, *J. Phys. Oceonol.*, **6**, 976–981.

Eckermann, Stephen, D., Isamu Hirota, and Wayne K. Hocking, 1995: Gravity wave and equatorial wave morphology of the stratosphere derived from long-term rocket soundings, *Quart. J. Roy. Meteor. Soc.*, **121**, 149–186.

——— and P. Preusse, 1999: Global measurements of stratospheric mountain waves from space, *Science*, **286**, 1534–1537.

Fetzer, E.J. and J.C. Gille, 1994: Gravity wave variance in LIMS temperature, Part I: Variability and comparison with background winds, *J. Atmos. Sci.*, **51**, 2461–2483.

Fritts, D.C., T. Tsuda, T. Sato, S. Fukao, and S. Kato, 1988: Observational evidence of a saturated gravity wave spectrum in the troposphere and lower stratosphere, *J. Atmos. Sci.*, **45**, 1741–1759.

——— and T.E. VanZandt, 1993: Spectral estimates of gravity wave energy and momentum fluxes, I, energy dissipation, acceleration and constraints, *J. Atmos. Sci.*, **50**, 3685–3694.

Gardner, C.S., C.A. Hosteler, and S.J. Franke, 1993: Gravity wave models for the horizontal wavenumber spectra of atmospheric velocity and density fluctuations, *J. Geophys. Res.*, **98**, 1035–1049.

Gorbunov, M.E. and L. Kornblueh, 2001: Analysis and validation of GPS/MET radio occultation data, *J. Geophys. Res.*, **106**, 17161–17169.

Hamilton, K., 1991: Climatological statistics of stratospheric inertia-gravity waves deduced from historical rocketsonde wind and temperature data, *J. Geophys. Res.*, **96**, 20831-20839.

Haugstad, B., 1981: *Spacecraft and stellar occultations by turbulent planetary atmospheres*: A theoretical investigation of various wave propagation effects and their impact on derived profiles of refractivity, temperature and pressure, NDRE/PUBL-81/1002, Norwegian Defense Research Establishment, Kjeller, Norway.

Hedin, A.E., 1991: Extension of the MSIS Thermospheric Model into the Middle and Lower Atmosphere, *J. Geophys. Res.*, **96**, 1159.

Hines, C.O., 1991: The saturation of gravity waves in the middle atmosphere, II, Development of Doppler spread theory, *J. Amos. Sci.*, **48**, 1360–1379.

Hinson, D.P. and G.L. Tyler, 1982: Spatial irregularities in Jupiter's upper ionosphere observed

by Voyager radio occultation, *J. Geophys. Res.*, **87**, 5275–5289.

——— and ———, 1983: Internal gravity waves in Titan's atmosphere observed by Voyager radio occultation, *ICARUS*, **54**, 337–352.

Hirota, I., 1984: Climatology of gravity waves in the middle atmosphere, *J. Atmos. Terr. Phys.*, **46**, 767–773.

Hocke, K., 1997: Inversion of GPS meteorology data, *Ann. Geophys.*, **15**, 443–450.

Holton, J., M. Alexander, and M. Boehm, 2001: Evidence for short vertical wavelength Kelvin waves in the doe-arm Nauru99 radiosonde data, *J. Geophys. Res.*, in press.

Jiang, J.H. and D.L. Wu, 2001: UARS MLS observations of gravity waves associated with the Arctic winters stratospheric vortex, *Geophys. Res. Lett.*, **28**, 527–530.

Karayel, E.T. and D.P. Hinson, 1997: Sub-Fresnel-scale vertical resolution in atmospheric profiles from radio occultation, *Radio Sci.*, **32**, 411–423.

Kursinski, E.R., G.A. Hajj, J.T. Schofield, R.P. Linfield, and K.R. Hardy, 1997: Observing Earth's atmosphere with radio occultation measurements using the Global Positioning System, *J. Geophys. Res.*, **102**, 23429–23465.

McLandress, C., M.J. Alexander, and D.L. Wu, 2000: Microwave limb sounder observations of gravity waves in the stratosphere: a climatology and interpretation, *J. Geophys. Res.*, **105**, 11947–11967.

Murayama, Y., T. Tsuda, and S. Fukao, 1994: Seasonal variation of gravity wave activity in the lower atmosphere observed with the MU radar, *J. Geophys. Res.*, **99**, 23057–23069.

Nastrom, G.D., A.R. Hansen, T. Tsuda, M. Nishida, and R. Ware, 2000: A comparison of gravity wave energy observed by VHF radar and GPS/MET over central North America, *J. Geophys. Res.—Atmospheres*, **105**, 4685–4687.

Nishida, M., T. Tsuda, C. Rocken, and R.H. Ware, 2000: Seasonal and longitudinal variations in the tropical tropopause observed with the GPS occultation technique (GPS/MET), *J. Meteor. Soc. Japan*, **78**, 691–700.

Palmer, P.I. and J.J. Barnett, 2001: Application of an optimal estimation inverse method to GPS/MET bending angle observations, *J. Geophys. Res.*, **106**, 17147–17160.

Preusse, P., B. Schaeler, J. Bacmeister, and D. Offermann, 1999: Evidence for gravity waves in CRISTA temperatures, *Adv. Space Res.*, **24**, 1601–1604.

———, S. Eckermann, and D. Offermann, 2000: Comparison of global distributions of zonal-mean gravity wave variance inferred from different satellite instruments, *Geophys. Res. Lett.*, **27**, 3877–3880.

Rocken, C., R. Anthes, M. Exner, D. Hunt, S. Sokolovskiy, R. Ware, M. Gorbunov, W. Schreiner, D. Feng, B. Herman, Y.-H. Kuo, X. Zou, 1997: Analysis and validation of GPS/MET data in the neutral atmosphere, *J. Geophys. Res.*, **102**, 29849–29866.

Shimizu, A. and T. Tsuda, 1997: Characterisctics of Kelvin waves and gravity waves observed with radiosondes over Indonesia, *J. Geophys. Res.*, **102**, 26159–26171.

Smith, S.A., D.C. Fritts, and T.E. VanZandt, 1987: Evidence of a saturation spectrum of atmospheric waves, *J. Atmos. Sci.*, **44**, 1404–1410.

Steiner, A.K. and G. Kirchengast, 2000: Gravity wave spectra from GPS/MET occultation observations, *J. Atmos. Ocean Tech.*, **17**, 495–503.

Tsuda, T., T. Inoue, D.C. Fritts, T.E. VanZandt, S. Kato, T. Sato, and S. Fukao, 1989: MST radar observations of a saturated gravity wave spectrum, *J. Atmos. Sci.*, **46**, 2440–2447.

———, T.E. VanZandt, M. Mizumoto, S. Kato, and S. Fukao, 1991: Spectral analysis of temperature and Brunt-Vaisala frequency fluctuations observed by radiosondes, *J. Geophys. Res.*, **96**, 17265–17278.

———, Y. Murayama, T. Nakamura, R.A. Vincent, A.H. Manson, C.E. Meek, and R.L. Wilson, 1994: Variations of the gravity wave characteristics with height, season and latitude revealed by comparative observations, *J. Atmos. Solar-Terr. Phys.*, **56**, 555–568.

———, M. Nishida, C. Rocken, and R.H. Ware, 2000: A global morphology of gravity wave activity in the stratosphere revealed by the GPS occultation data (GPS/MET), *J. Geophys. Res.*, **105**, 7257–7273.

Ware, R., M. Exner, D. Feng, M. Gorbunov, K. Hardy, B. Herman, Y. Kuo, T. Meehan, W. Melbourne, C. Rocken, W. Schreiner, S. Sokolovskiy, F. Solheim, X. Zou, R. Anthes, S. Businger, and K. Trenberth, 1996: GPS sounding of the atmosphere From Low Earth Orbit: Preliminary Results, *Bull. Am. Meteor. Soc.*, **77**, 19–40.

Wu, D.L. and J.W. Waters, 1996a: Gravity-wave-scale temperature fluctuations seen by UARS MLS, *Geophys. Res. Lett.*, **23**, 3289–3292.

——— and J.W. Waters, 1996b: Satellite observations of atmospheric variances: A possible indication of gravity waves, *Geophys. Res. Lett.*, **23**, 3631–3634.